A Dual-Wavelength Fiber Ring Laser Incorporating an Injection-Coupled Optoelectronic Oscillator and Its Application to Transverse Load Sensing

Fanqi Kong, *Student Member, IEEE*, Bruno Romeira, *Member, IEEE*, Jiejun Zhang, *Student Member, IEEE*, Wangzhe Li, *Student Member, IEEE*, and Jianping Yao, *Fellow, IEEE, Fellow, OSA*

***Abstract*—A novel configuration for a dual-wavelength fiber ring laser with improved lasing stability realized through the use of an injection-coupled optoelectronic oscillator (OEO) is proposed and demonstrated, and its application to transverse load sensing is studied. The OEO-coupled dual-wavelength laser has two mutually coupled loops: the fiber ring loop and the OEO loop. In the fiber ring loop, a polarization-maintaining phase-shifted fiber Bragg grating is incorporated to generate two optical wavelengths with the wavelength spacing determined by the birefringence of the polarization-maintaining (PM) fiber. In the OEO loop, a microwave signal with its frequency also determined by the birefringence of the PM fiber is generated, which is fed into the fiber ring loop to injection lock the dual wavelengths. Due to the injection locking, a very stable dual-wavelength operation is established. The use of the dual wavelengths for high-resolution and high-speed transverse load sensing is then implemented. The sensitivity of the transverse load sensor is measured as high as +9.7573 and −9.7350 GHz/(N/mm), along the fast and slow axes, respectively. The high frequency purity and stability of the generated microwave signal permits very reliable and high accuracy measurement and the microwave frequency interrogation allows the system to operate at an ultra-high speed.**

***Index Terms*—Dual-wavelength laser, fiber laser, fiber optic sensor, laser stability, microwave photonics (MWP), microwave signal generation, optoelectronic oscillator (OEO).**

I. Introduction

DUAL-WAVELENGTH lasers are used for a wide variety of applications such as in secure communications [1], ranging [2], high-resolution interferometry [3], optical sensing [4], and microwave photonic (MWP) signal generation [5]. Such applications can take advantage of the inherent properties of a fiber laser such as high power, narrow linewidth, and high signal-to-noise ratio (SNR). The compatibility with other fiber optic devices and systems is another significant advantage. The lasing wavelengths are selected usually by using an optical filter. Among the many types of optical filters, a fiber Bragg grating (FBG) is an ideal wavelength selection component thanks to the simplicity, low loss, small size and low cost characteristics. Different techniques to implement a dual-wavelength fiber laser based on FBGs have been demonstrated in the last few years, such as the use of cascaded FBGs [6], an FBG written in a birefringent fiber [7], a sampled FBG [8], [9], and a linear Fabry-Perot cavity composed of two FBGs [10]. Two independent optical longitudinal modes as well as their heterodyning electrical signal can be generated, which can be employed for both signal generation and sensing.

Optical sensors based on FBGs [11], [12] have been proposed and widely applied in numerous fields such as structural health monitoring [13], [14], medical treatment [15] and pipeline security monitoring [16]. The sensing information encoded in an FBG due to the structural distortion [17], [18] can be interrogated through measuring its optical characteristics. The birefringence, in particular, as a key optical characteristic describing the anisotropy of an FBG along the two principal axes in terms of the refractive indices, provides an important measurement to the lateral external disturbance such as bending, pressing, and twisting [19], [20]. Among the various physical quantities that can be measured through monitoring the change of the birefringence, the transverse load is a vital parameter in structural health monitoring, which can be ideally measured through the non-axisymmetric load induced birefringence [21], [22]. However, the lateral force-induced refractive change is very small, thus a specially designed interrogation technique must be employed to demodulate the sensing information.

The change in birefringence can be measured based on time-domain intensity analysis [23], spectral domain optical wavelength analysis [21], and the electrical frequency analysis [11], [22], [24]. The time-domain approach is usually faster than the spectral domain approach, but with its own limitation. For example, the time-domain intensity analysis approach can implement birefringence measurement in real-time. The major limitation of the approach in [23] is that only the phase retard can be demodulated, which is not uniquely associated with absolute value of the induced birefringence due to the periodicity of the intensity profile, which is also easily to be affected by undesired environment fluctuations. The absolute value of a force-induced birefringence change can be measured

Manuscript received December 29, 2013; revised March 5, 2014; accepted March 10, 2014. Date of publication March 12, 2014; date of current version April 10, 2014. This work was supported by the Natural Sciences and Engineering Research Council of Canada.

F. Kong, J. Zhang, W. Li, and J. Yao are with the Microwave Photonics Research Laboratory, School of Electrical Engineering and Computer Science, University of Ottawa, Ottawa, ON K1N 6N5, Canada (e-mail: jpyao@eecs.uottawa.ca).

B. Romeira is with the Microwave Photonics Research Laboratory, School of Electrical Engineering and Computer Science, University of Ottawa, Ottawa, ON K1N 6N5, Canada and also with the Center of Electronics Optoelectronic and Telecommunications, Department of Physics, University of the Algarve, 8005-139 Faro, Portugal.

Color versions of one or more of the figures in this paper are available online at http://ieeexplore.ieee.org.

Digital Object Identifier 10.1109/JLT.2014.2311799

based on the spectral-domain wavelength analysis approach using an optical spectrum analyzer (OSA). If the resolution of the OSA is sufficiently high, the two spectral peaks can be resolved. However, since the optical spectrum measurement is a slow process, the approach is not suitable for high-speed applications. In addition, the lateral force induced birefringence change is very small, thus an OSA with an ultra-high resolution should be used, which will significantly increase the cost. To avoid the use of an ultra-high resolution OSA, a solution is to incorporate a birefringence FBG in a fiber laser to generate two wavelengths. By measuring the frequency of the beat note in the electrical domain, high-speed and ultra-high resolution interrogation can be achieved [25]. The key limitation of a dual-wavelength fiber laser for high-resolution sensing is the instability due to the strong wavelength competition at room temperature. Recently we proposed a technique to interrogate a birefringence sensor using an optoelectronic oscillator (OEO) incorporating a polarization-maintaining phase-shifted FBG (PM-PSFBG). Due to the phase-modulation to intensity-modulation (PM-IM) conversion in the PM-PSFBG [26], a dual-passband microwave filter with a frequency spacing between the two passbands determined by the wavelength of the optical carrier and the two notch wavelengths is formed, which leads to the generation of two microwave signals in the electrical domain. A third signal that is the beat note between the two microwave signals due to the nonlinearity of the OEO loop is generated. The frequency of the beat note is directly related to the force-induced birefringence [22]. It is different from optical amplification in which strong homogenous line broadening would increase the wavelength competition, electrical amplification has no such effect, and the stability of the dual-frequency OEO is significantly improved. The major limitation of the OEO-based approach is the possible frequency measurement ambiguity. The frequency of the beat note is not always the lowest frequency, thus it is critical to identify correctly the beat frequency to make a correct measurement.

In this paper, we propose a dual-wavelength fiber ring laser incorporating an injection-coupled OEO, to generate a stable microwave signal. By encoding the sensing information in the microwave frequency, the dual-wavelength fiber laser can be employed as a transverse load sensor. Since only a single microwave frequency is generated, the ambiguity problem in the OEO-based approach in [22] is avoided.

The proposed fiber-optic sensor has two mutually coupled loops, the fiber ring loop and the OEO loop. A PM-PSFBG is incorporated in the two loops. In the fiber ring loop, the use of the PM-PSFBG would generate two optical wavelengths with the wavelength spacing determined by the birefringence of the polarization-maintaining fiber (PMF). In the OEO loop, a microwave signal with its frequency also determined by the birefringence of the PMF is generated, which is fed back into the fiber ring loop to injection-lock the dual wavelengths. Due to the injection locking, a very stable dual-wavelength operation is reached. The beating between the dual wavelengths generates a microwave signal which is used to implement high-speed and high-resolution transverse load sensing. The high spectrum purity and high stability of the generated microwave signal permits very reliable and high accuracy measurement, and the time-domain frequency measurement allows the interrogation at an ultra-high speed. An experiment is performed. A dual-wavelength fiber ring laser with an ultra-stable operation is demonstrated. The use of the fiber ring laser to perform transverse load sensing is also demonstrated. A sensitivity as high as +9.7535 and −9.7350 GHz/(N/mm), along the fast and slow axes, respectively, is realized.

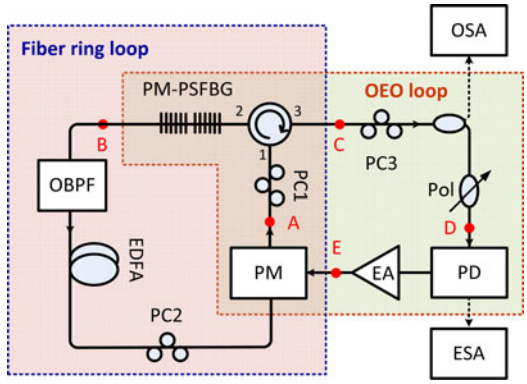

Fig. 1. (Color online) The schematic of the proposed dual-wavelength fiber ring laser incorporating an injection-coupled OEO. PM: phase modulator; PC: polarization controller; PD: photodetector; EA: electrical amplifier; PM-PSFBG: polarization maintaining phase-shifted fiber Bragg grating; OBPF: optical bandpass filter; Pol: polarizer; OSA: optical spectrum analyzer; ESA: electrical spectrum analyzer; EDFA: erbium-doped fiber amplifier.

II. Principle

The schematic diagram of the dual-wavelength fiber ring laser incorporating an injection-coupled OEO is shown in Fig. 1. As can be seen the OEO-coupled dual-wavelength fiber ring laser consists of two mutually coupled loops, the fiber ring loop and the OEO loop. A path consisting of a phase modulator (PM) and a PM-PSFBG are shared by the two loops. For the fiber ring loop, the lasing is established due to the gain of the erbium-doped fiber amplifier (EDFA). The dual wavelength selection is realized due to the dual passbands of the PM-PSFBG along the two principal axes. For the OEO, the oscillation is started due to the gain from the electrical amplifier (EA). The oscillation frequency is determined by the central frequency of an equivalent microwave filter formed due to the PM-IM conversion in the PM-PSFBG. The generated microwave signal is re-injected into the fiber ring cavity at the PM, which is the key to improve the stability of the fiber ring laser.

A. Fiber Ring Loop

The fiber ring loop consists of an EDFA, a PM-PSFBG serving as a dual-wavelength polarization-dependent optical filter, an OBPF, a PM, and two polarization controllers (PC1 and PC2). In the system, the PM supports phase modulation only along one polarization direction.

The PM-PSFBG is the key device in the fiber ring loop that ensures dual wavelength operation. In fact, the PM-PSFBG is written in a PMF with a phase shift introduced into the grating during the fabrication. Due to the birefringence of the PMF, the

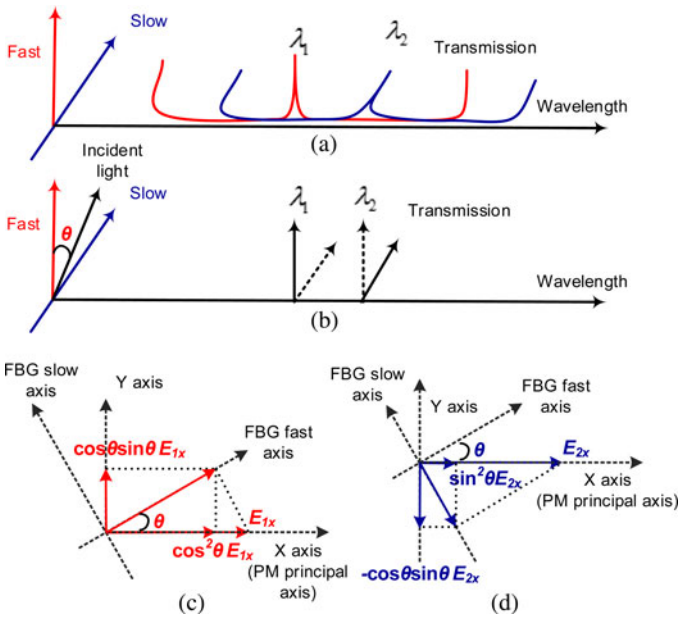

Fig. 2. (a) The transmission bands along the fast and slow axes of the PM-PSFBG. (b) The light waves at λ_1 and λ_2 are transmitted, respectively, along the fast and slow axes of the PM-PSFBG (solid arrows). (c) The light wave at λ_1 is transmitted through the fast axis of the PM-PSFBG and then projected to the x axis which is also the principal axis of the PM. (d) The light wave at λ_2 is transmitted through the slow axis of the PM-PSFBG and then projected to the x axis.

refractive indices along the two principal axes are slightly different, which lead to two ultra-narrow and slightly separated transmission bands at λ_1 and λ_2. The incorporation of the PM-PSFBG into the fiber ring loop would lead to the generation of two orthogonally polarized light waves at λ_1 and λ_2 with each operating in the single-longitudinal mode due to the ultra-narrow width of each of the transmission bands.

Assuming that the light wave at point A is the summation of two light waves with their wavelengths at λ_1 and λ_2, the complex amplitude of the electric field of the light wave can be described by a Jones vector. Since the PM supports phase modulation along only one polarization direction (x axis, the principal axis of the PM), only the components in the Jones vector along the x axis have non-zero values, E_{1x} and E_{2x}, which are the complex amplitude along principal axis of the PM corresponding to the lasing wavelengths λ_1 and λ_2. The total electric field at point A, as shown in Fig. 1, is given by

$$E_A = \begin{bmatrix} E_{1x} \\ 0 \end{bmatrix} + \begin{bmatrix} E_{2x} \\ 0 \end{bmatrix}. \tag{1}$$

The light is linearly polarized, which is sent to the PM-PSFBG through a polarization controller (PC1). The PM-PSFBG has two ultra-narrow transmission bands along the two principal axes, as shown in Fig. 2(a). The polarization direction of the light wave is controlled by PC1 to have an angle of θ relative to the fast axis of the PM-PSFBG, as shown in Fig. 2(b).

For the light wave at λ_1, it is incident to the PM-PSFBG with an angle of θ relative to the fast axis, thus it is split into two orthogonal components, with the one along the fast axis transmitted through the transmission band at λ_1 and the component projected to the slow axis is reflected, as shown in Fig. 2(c). For the light wave at λ_2, the component projected to the slow axis is transmitted through the transmission band at λ_2 and the component projected to the fast axis is reflected as shown in Fig. 2(d). Thus, the total electric field after the PM-PSFBG at point B is given by

$$E_B = \begin{bmatrix} \cos^2(\theta) E_{1x} \\ \sin(\theta)\cos(\theta) E_{1x} \end{bmatrix} + \begin{bmatrix} \sin^2(\theta) E_{2x} \\ -\sin(\theta)\cos(\theta) E_{2x} \end{bmatrix}. \tag{2}$$

Since the PM only supports phase modulation along the x direction, the powers of the light waves along the x direction for the two wavelengths at λ_1 and λ_2 can be adjusted by tuning the angle θ, as can be seen from (2). For example, when $\theta = 0$, the light wave at λ_1 is transmitted, and the light wave at λ_2 is reflected. In this case, a single-wavelength lasing at λ_1 will be supported. When $\theta = \pi/2$, the light wave at λ_2 will be transmitted while the light wave at λ_1 is reflected. In this case, a single-wavelength lasing at λ_2 will be supported. The laser can also work in a dual-wavelength mode if the powers for the two wavelengths are balanced by tuning PC2. Due to the strong wavelength competition in the gain medium, the operation in a dual-wavelength mode is not stable. A solution to improve the stability is to introduce an OEO into the system. Through injection locking of the two wavelengths, the stability can be improved.

B. OEO Loop

The OEO loop is formed by the PM-PSFBG, the PM, a polarizer (Pol), a PD, an EA, and two PCs (PC1 and PC3). The PM-PSFBG and the PM are shared with the fiber ring loop. In the OEO loop, the PM-PSFBG is operating in the reflection mode with two ultra-narrow notches along the fast and slow axes, as shown in Fig. 3(a). The light wave at λ_1 projected to the slow axis is reflected into the OEO loop, and the light wave at λ_2 projected to the fast axis is reflected into the OEO loop, as shown in Fig. 3(b).

Again, the total electric field consisting of the two reflected light waves at λ_1 and λ_2 at point C is given by

$$E_C = \begin{bmatrix} \sin^2(\theta) E_{1x} \\ -\sin(\theta)\cos(\theta) E_{1x} \end{bmatrix} + \begin{bmatrix} \cos^2(\theta) E_{2x} \\ \sin(\theta)\cos(\theta) E_{2x} \end{bmatrix}. \tag{3}$$

The two light waves are sent to the PD through a polarizer to project the two orthogonally polarized light waves to the principal axis of the polarizer, and beat them at the PD. If the principal axis of the polarizer is oriented at an angle $\varphi = \theta$-$\pi/4$ relative to the principal axis of the PM, as shown in Fig. 3(c), we have the total electric field along the principal axis of the polarizer, given by

$$\begin{aligned} E_D &= \begin{bmatrix} \cos(-\varphi) & -\sin(-\varphi) \\ 0 & 0 \end{bmatrix} E_C \Big|_{\varphi=\theta-\frac{\pi}{4}} \\ &= \frac{\sqrt{2}}{2}\left[\sin(\theta)E_{1x}\cos(\omega_1 t) + \cos(\theta)E_{2x}\cos(\omega_2 t)\right] \end{aligned} \tag{4}$$

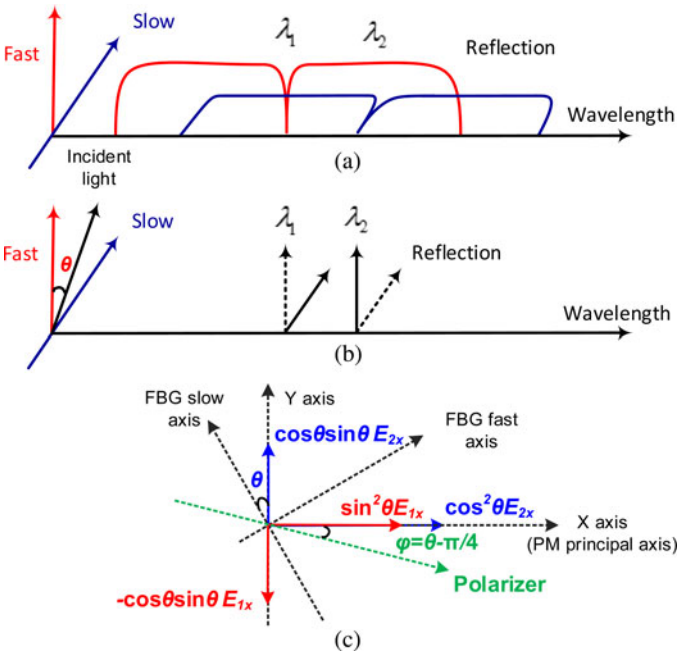

Fig. 3. (Color online) (a) The reflection bands along the fast and slow axes of the PM-PSFBG. (b) The light waves at λ1 and λ2 are reflected by the PM-PSFBG, respectively, along the slow and fast axes of the PM-PSFBG. (c) The principal axis of the polarizer is oriented at an angle of $\varphi = \theta - \pi/4$ relative to the principal axis of the PM.

where ω_1 and ω_2 are the angular frequencies of the light waves at λ_1 and λ_2. The photo current at the output of the PD is given by

$$i_{\mathrm{PD}} = R\left|E_D\right|^2 = \frac{1}{4}R\sin(2\theta)\,E_{2x}E_{1x}\cos\left[(\omega_1-\omega_2)\,t\right] = I_{\mathrm{PD}}\cos(\Omega t) \quad (5)$$

where R is the responsivity of the PD, $I_{\mathrm{PD}} = \frac{1}{4}R\sin(2\theta)E_{2x}E_{1x}$ is the amplitude of the ac component, and Ω is the angular frequency of the detected microwave signal. Note that in deriving (5), the dc component is ignored.

After amplification by an EA with a gain of G_{EA}, we have the output microwave signal at point E in Fig. 1. The amplitude voltage of the microwave signal is given by

$$V_E = L_E G_{\mathrm{EA}} Z_L I_{\mathrm{PD}} = \frac{1}{4}L_E G_{\mathrm{EA}} \mathrm{R} Z_L \sin(2\theta)\,E_{2x}E_{1x} \quad (6)$$

where L_E is the total insertion loss in the OEO loop, Z_L is the load impedance, and G_{EA} is the voltage gain of the EA.

The signal from the EA is sent back to the PM to close the OEO loop, at the same time, as an injection signal to injection lock the two wavelengths of the fiber ring laser.

C. OEO-Coupled Dual-Wavelength Fiber Ring Laser

The mutual coupling between the two loops to stabilize the operation of the dual-wavelength fiber ring laser is analyzed. The dual-wavelength operation in the fiber ring laser is very unstable due to the homogenous line broadening in the gain medium which leads to strong wavelength competition. The stability can be significantly improved if an OEO loop is incorporated into the fiber ring laser.

We start our analysis by considering first only one lasing wavelength, say λ_1, as the optical carrier for the OEO, which corresponds to $\theta = 0$. When the OEO loop is closed, microwave oscillation will start. The frequency of the generated microwave signal is determined by the wavelength of the optical carrier at λ_1 and the central wavelength of the notch. Since the PM only supports phase modulation along the x direction, generally, the electric field of the phase-modulated signal at the output of the PM is given by

$$E_{\mathrm{PM}}(t) = E_{1x}\exp\left\{j\left[\omega_1 t + \pi\frac{V_E}{V_\pi}\cos(\Omega t)\right]\right\} \approx E_{1x}\sum_{n=0,\pm1}(-1)^n J_n(\beta)\exp\left[j(\omega_1 t + n\Omega t)\right] \quad (7)$$

where E_{PM} is the electric field at the output of the PM (point A in Fig. 1) along the x direction, E_{1x} and ω_1 are, respectively, the electric field and the angular frequency of the optical carrier along the x direction, V_E is the amplitude voltage of the microwave signal at the output of the EA (point E in Fig. 1), V_π is the half-wave voltage of the PM, $\beta = \pi V_E/V_\pi$ is the modulation index, $J_n(\beta)$ is the Bessel function of the first kind of an order n, and Ω is the angular frequency of the modulation microwave signal. If we directly detect the phase-modulated signal at the PD, due to out-of-phase nature of the $+1^{\mathrm{st}}$ and -1^{st} order sidebands, the beating between optical carrier and the $+1^{\mathrm{st}}$ order sideband will completely cancel the beating between optical carrier and the -1^{st} order sideband. However, if the phase-modulated signal is directed to the PM-PSFBG, one sideband at λ_2 is filtered out and a single-sideband with carrier (SSB+C) signal is thus generated. The detection of the SSB+C signal at the PD will produce a microwave signal [26], [27], which then is amplified by the EA and sent back to the PM to close the OEO loop. If the gain is greater than the total loss in the OEO loop, self-sustained oscillation will be established and a microwave signal will be generated.

If θ is adjusted such that dual-wavelength lasing is established. The stable operation of the dual wavelengths is due to the mutual injection locking. For example, for the wavelength at λ_1, the phase modulated signal has a sideband that is exactly located at the other transmission band of the PM-PSFBG at λ_2, thus the sideband at λ_2 will be injected into the fiber ring laser. Such injection provides extra energy to λ_2, which helps to initialize lasing. The two wavelengths will finally reach a steady state, due to the nonlinear effect in both the gain medium and the PM, in which the electric field at any point of the ring loop after a round trip should keep constant. The complex amplitude after a round trip at the output of the PM (point A in Fig. 1) can be derived as

$$E'_{1A} = L_O G(E_{1x}, E_{2x})\begin{bmatrix}1 & 0\\ 0 & 0\end{bmatrix}\{J_0(\beta)E_{1B} + J_{-1}(\beta)E_{2B}\} \quad (8a)$$

$$E'_{2A} = L_O G(E_{1x}, E_{2x})\begin{bmatrix}1 & 0\\ 0 & 0\end{bmatrix}\{J_0(\beta)E_{2B} + J_1(\beta)E_{1B}\} \quad (8b)$$

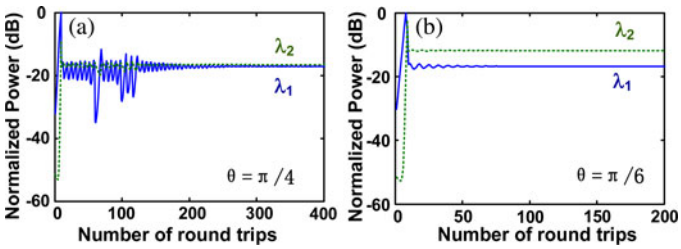

Fig. 4. Simulation results. (a) The normalized optical powers for λ_1 (solid line) and λ_2 (dashed line) versus the number of round trips, with an incident angle of $\theta = \pi/4$. (b) The normalized optical powers for λ_1 (solid line) and λ_2 (dashed line) versus the number of round trips, with an incident angle of $\theta = \pi/6$.

where E'_{1A}, E'_{2A}, represent the complex amplitudes for λ_1 and λ_2 at point A after a round trip; L_O is the total insertion loss in the optical fiber ring loop, $G(E_{1x}, E_{2x})$ is the nonlinear gain of the optical gain medium which is a function of the input optical power. E_{1B} and E_{2B} are two 1×2 Jones vectors of the complex amplitudes at point B given in (2) for λ_1 and λ_2, respectively. The 2×2 matrix $\left[\begin{smallmatrix}1 & 0\\ 0 & 0\end{smallmatrix}\right]$ represents an equivalent linear polarizer along the x direction, since only the light wave along the x direction is modulated at and transmitted through the PM. Again, $J_n(\beta)$ is the Bessel function given in (7).

By applying the self-consistency condition, $E'_{1A}{=}E_{1A}$ and $E'_{1A}{=}E_{1A}$, and substituting the complex amplitudes of electric field at point B into (8a) and (8b), the complex amplitudes in the steady state are given by

$$E_{1x} = \alpha G(E_{1x}, E_{2x}) \left\{ J_0(\beta) \cos^2(\theta) E_{1x} + J_{-1}(\beta) \sin^2(\theta) E_{2x} \right\} \tag{9a}$$

$$E_{2x} = \alpha G(E_{1x}, E_{2x}) \left\{ J_0(\beta) \sin^2(\theta) E_{2x} + J_1(\beta) \cos^2(\theta) E_{1x} \right\}. \tag{9b}$$

In (9a), the first term in the braces corresponds to the remained zero-order light wave at λ_1 and the second term represents the contribution of the injected sideband from λ_2. In (9b), the first term in the braces corresponds to the remained zero-order light wave at λ_2 and the second term represents the contribution of the injected sideband from λ_1. Such mutual injection locking will help stabilize the dual-wavelength operation.

The mutual injection locking to stabilize the dual wavelength lasing is simulated. In the simulation, the incident angle to the PM-PSFBG is set at two different values, $\theta = \pi/4$ and $\theta = \pi/6$. The power of λ_1 is set to be 20 dB stronger than that of λ_2 in the initial condition. The simulation results are shown in Fig. 4. As can be seen the two wavelengths reach a steady state after several round trips for both cases.

It can be seen that in the first few round trips, the higher initial power of λ_1 will make its power increase and the power of λ_2 decrease dramatically due to the mode competition. However, immediately after the first few round trips, in the next tens of round trips, the nonlinear effect of the modulation and OEO injection restrain the mode competition and bring up the power of λ_2: the decreasing optical power at λ_2 will reduce its -1^{st} order sideband accordingly, which will lead to the reduction in the optical power injected into λ_1. Simultaneously, the increasing λ_1 will induce a stronger injection to λ_2, which counteracts the effect of mode competition. Such reciprocating power vibration of the two wavelengths will finally reach a steady state with a power ratio between the two wavelengths depending on the incident angle θ. Such effect induced by the mutual injection can improve the system stability with an increased tolerance to an imbalanced initial condition.

D. Transverse Load Sensing

Since a very stable dual-wavelength lasing is reached, the fiber ring laser can be used for sensing applications. The frequency of the microwave signal generated in the OEO-coupled dual-wavelength laser is only determined by the spacing between the dual wavelengths, which is a function the birefringence of the PM-PSFBG. If a transverse load is applied to the PM-PSFBG, the beat frequency between the two wavelengths will shift due to the change in the birefringence [12], [21]. The frequency spacing between the two notches along the two principal axes is given by [12]

$$\Omega = \omega_1 - \omega_2 = \frac{c}{n_0 \lambda_1} B \tag{10}$$

where ω_1, ω_2 are the frequencies corresponding to λ_1 and λ_2, n_0 is the averaging refractive index of the fiber, B is the load-induced birefringence, given by [22]

$$B = \frac{2 n_0^3 (p_{11} - p_{12})(1 + \nu_p) \cos(2\varphi) F}{\pi r \varepsilon} \tag{11}$$

where p_{11} and p_{12} are the components of the strain-optical tensor of the optical material, ν_p is Poisson's ratio, ε is the Young's modulus of the fiber, r is the radius of the fiber, φ is the angle between the direction of the force and the slow axis of the fiber, and F is the linear transverse load (force per unit length) [12], [28]. By measuring the frequency of the microwave signal, the transverse force applied to the fiber can be interrogated. It is noteworthy to mention that the sensitivity of the transverse load sensor is directly related to the angle of the force applied to the fiber. Only when the angle of force is 0 or $\pi/2$, in other words, the direction of the force is aligned with either the slow or fast axis of the fiber, a maximum sensitivity can be reached.

III. Experiment

In the experiment, we first study the operation of the proposed dual-wavelength fiber ring laser incorporating an injection-coupled OEO. Then, its application for high-resolution and high-speed transverse load sensing is investigated.

A. Optical Carrier Generation

We first demonstrate the fiber ring laser to operate for the generation of a single wavelength and dual wavelengths. The ultra-narrow transmission bands of the PM-PSFBG are used to select the lasing wavelengths. The PM-PSFBG is fabricated in a PMF using a chirped phase mask that is illumined by a UV light.

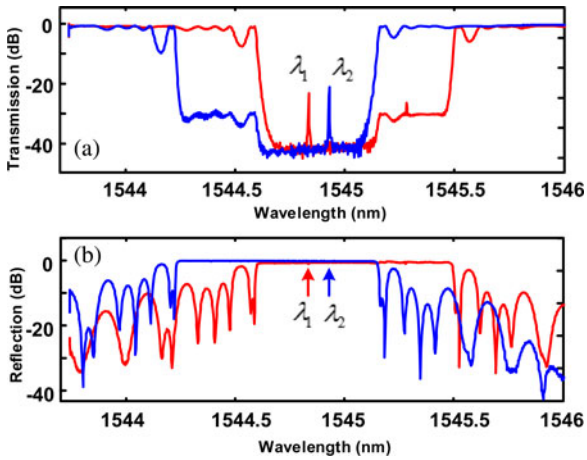

Fig. 5. (Color online) (a) The normalized transmission spectra of the PM-PSFBG along the two principal axes. (b) The normalized reflection spectra of the PM-PSFBG along the two principal axes.

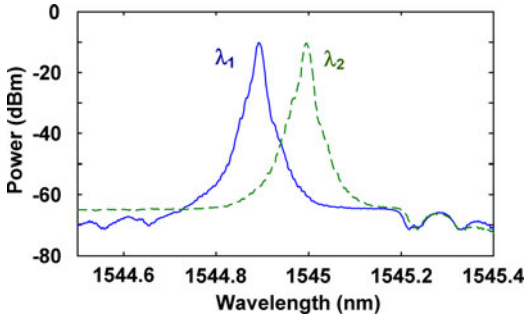

Fig. 6. The optical spectrum of the light wave generated by the fiber ring laser at λ_1 (solid line) or λ_2 (dashed line).

The phase shift in the grating is introduced by laterally moving the phase mask during the fabrication. The transmission and the reflection spectra of the PM-PSFBG along the two principal axes are measured by an optical vector analyzer (OVA, LUNA Technologies) which are shown in Fig. 5. As can be seen the PM-PSFBG has a reflectivity of over 99.99% for the two reflection bands. In Fig. 5(a), the bottom of the transmission spectra has a step, which is caused by a slight misalignment of the polarization direction of the incident light to one principal axis, leading the coupling of the light to the direction of the other principal axis. In the reflection spectra shown in Fig. 5(b), the narrow notches cannot be resolved due to the limited resolution of the OVA. The 3-dB reflection bandwidths of the PM-PSFBG along the two principal axes are measured to be 117.3 and 113.3 GHz.

To guarantee that the laser is operating at the narrow transmission bands of the PM-PSFBG, an optical bandpass filter (OBPF, Finisar WaveShaper 4000S) of a bandwidth of 50 GHz is inserted in the fiber ring loop to select the two transmission bands, as shown in Fig. 1. If the gain provided by the EDFA (Nortel FA17UFAC-119C28) is sufficiently large to fully compensate for the loss in the fiber ring loop, including the polarization induced coupling loss at the PM-PSFBG, the laser will start to lase. The minimum output power of the EDFA to ensure stable lasing is 11 dBm. In the experiment, to generate a microwave signal with a good SNR at the output of the PD, the output power of the EDFA is set to be 15 dBm. In this case, the output power of the laser is measure to be -3 dBm.

As shown in (2), depending on the polarization direction of the light wave relative to the fast axis of the PM-PSFBG, the laser can operate at a single wavelength or dual wavelengths. For example, if the incident angle θ is tuned to be equal to 0° or 90°, the transmission of λ_1 or λ_2 is maximized, and the laser will operate at a single wavelength at λ_1 or λ_2. If the incident angle θ is tuned to balance the transmissions at λ_1 and λ_2, then the laser will operate at dual wavelengths. Note that the tuning is done by tuning PC1 in the experiment. Fig. 6(a) shows the spectrum at the output of the fiber ring laser corresponding to a single wavelength operation at λ_1 or λ_2. As can be seen the two wavelengths are at 1544.895 and 1544.993 nm with a wavelength spacing of 0.098 nm and a sideband suppression ratio of 50 dB for both wavelengths. To verify that the laser is operating in single longitudinal mode, we apply the light wave from the fiber ring laser to a PD and monitor the spectrum using an electrical spectrum analyzer (ESA). No beat notes are observed which confirms that the fiber ring laser is operating in single longitudinal mode. In the measurement, the loop length of the fiber laser is about 50 m. Note that the single longitudinal mode operation will not be maintained if the loop length is increased to 500 m. In the experiment, when the loop length is increased greater than 500 m, multiple longitudinal modes would be observed, although the total output power of the laser is kept unchanged.

B. OEO Operation With a Single Optical Carrier

The OEO operation with a single wavelength from the fiber ring laser as an optical carrier to support the OEO oscillation is investigated. The incident angle θ is controlled such that the ring laser is operating at a single wavelength, which is coupled into the OEO loop to serve as the optical carrier. In the experiment, we tune the incident angle θ via tuning PC1 to make the laser operate at λ_1 of 1544.895 nm. Due to the PM-IM conversion at the PM-FSFBG, the phase-modulated signal is converted to an SSB+C signal [27], which is detected by the PD (New Focus 10058B, 20 GHz). The optical spectrum of the SSB+C signal is measured by an optical spectrum analyzer (OSA, ANDO 6317B), which is shown in Fig. 7. As can be seen the $+1^{\text{st}}$ order sideband at 1544.993 nm is suppressed by 8 dB. The detected electrical signal is sent to the EA (6–18 GHz, NARDA 60583). After amplification by the EA, the electrical signal is sent back to the PM to close the OEO loop. The joint operation of the PM and the PM-PSFBG is equivalent to a MWP filter [26]. The frequency response of the equivalent MWP filter is measure by a vector network analyzer (VNA, Agilent E8364A), which is shown in Fig. 7(b). As can be seen the MWP filter has a passband centered at 11.8 GHz with a bandwidth of about 10 MHz. Thanks to the ultra-narrow passband of the equivalent MWP filter, a single-frequency oscillation in the OEO is achieved.

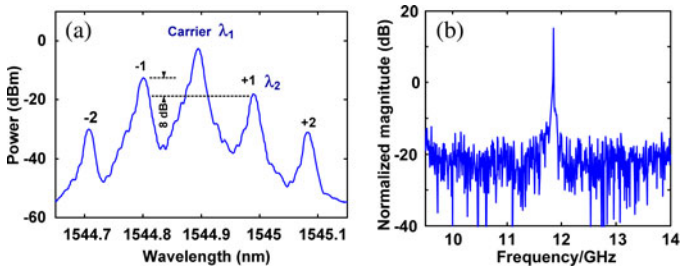

Fig. 7. (a) The optical spectrum of the SSB+C signal measured at port 3 of the optical circulator by the OSA. The $+1^{st}$ order sideband is suppressed by 8 dB. (b) The magnitude response of the equivalent microwave photonic filter.

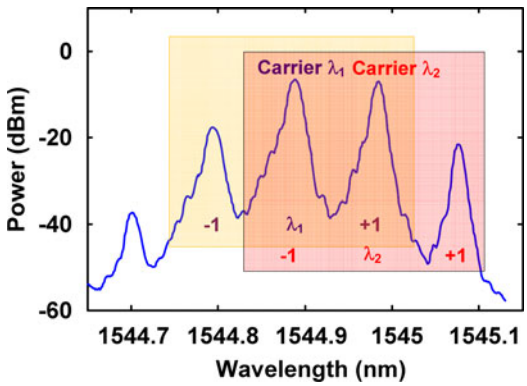

Fig. 8. The optical spectrum at the output of port 3 of the optical circulator when the fiber ring laser is operating to generate dual wavelengths.

C. OEO Operation With Dual Optical Carriers

The OEO operation with two wavelengths from the fiber ring laser is then investigated. The incident angle θ is controlled such that the fiber ring laser is operating at dual wavelengths. The optical spectrum measured at the port 3 of the optical circulator is shown in Fig. 8. As can be seen, each wavelength serving as an optical carrier to generate a double-sideband plus carrier (DSB+C) signal. Note that the DSB+C signal for the optical carrier at λ_1 has its $+1^{st}$ order sideband located at the optical carrier at λ_2, and the DSB+C signal for the optical carrier at λ_2 has its -1^{st} order sideband located at the optical carrier at λ_1. This is the mutual coupling, which is the key mechanism that ensures a stable operation of the dual-wavelength fiber ring laser. Thanks to this mechanism, the injection counteracts the effect of mode competition and stabilizes the dual-wavelength lasing.

D. Microwave Signal Generation

For the fiber ring laser to operate at both the single-wavelength and the dual-wavelength states, a microwave signal is generated by the OEO. Since the oscillating frequency is only determined by the birefringence of the PM-PSFBG, the frequency of the microwave signal is independent of the wavelength of the optical carrier or carriers from the fiber ring laser. However, the microwave signal generated, when the fiber ring laser is operating in the dual-wavelength state, has better signal quality. The reason is that the beating between the two optical carriers

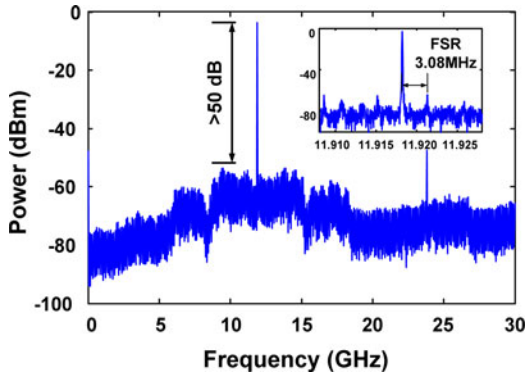

Fig. 9. The electrical spectrum of the microwave signal at the output of the PD.

provides higher signal power than the beating between the carrier and one sideband. Thus, the fiber ring laser is controlled to operate in the dual-wavelength state to perform the microwave signal generation experiment. By beating the two lasing wavelengths at the PD, a microwave signal at 11.8 GHz is generated. Note that the frequency of 11.8 GHz corresponds to the intrinsic birefringence of the PM fiber. Fig. 9 shows the spectrum of the generated microwave signal. The signal power can reach -3 dBm with a SNR over 50 dB, which can be easily detected and tracked by an electrical spectrum analysis device such as an ESA. A zoom-in view of the spectrum is shown as an inset in Fig. 9, which confirms the single-mode oscillation with a sidemode suppression ratio over 50 dB. The free spectrum range (FSR) is measured to be 3.08 MHz, which is consistent with the total length OEO loop of about 60 m. A second peak at 23.6 GHz is observed, which is the 2nd harmonic generated due to nonlinearity of the OEO loop.

E. Transverse Load Sensing

Considering the better quality of the microwave signal generated by the OEO for the fiber ring laser operating at the dual wavelength mode, in the experiment the fiber ring laser is configured to operate at the dual-wavelength mode to perform the sensing experiment.

A transverse load is applied to the PM-PSFBG through a glass plate. In the experiment, to ensure the system to reach its highest sensitivity, the transverse load is applied to the PM-PSFBG along its fast or slow axis. A supporting fiber with an identical radius is placed in parallel with the PM-PSFBG to guarantee that the load is applied to the PM-PSFBG transversely, while sharing half of the applied load, as shown in Fig. 10(a). To avoid non-uniformed mechanical elastic property of the post coating on the PM-PSFBG, an initial load is applied to the sensing probe in order to reach its linear response regime, which also helps to fix the fiber with a constant angle to the direction of the force when increasing or decreasing the load. By increasing the load applied to the PM-PSFBG, the beat frequency is shifted towards a higher frequency, as shown in Fig. 1(b), measured by an ESA, from 11.9033 to 12.3897 GHz with a load from 0 to 0.03969 N/mm.

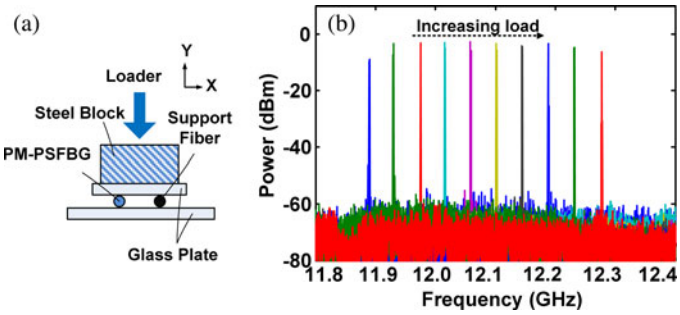

Fig. 10. (a) The setup for applying a transverse load to the PM-PSFBG. (b) The electrical spectrum of the microwave signal with increasing the load applied to the fast axis of the PM-PSFBG.

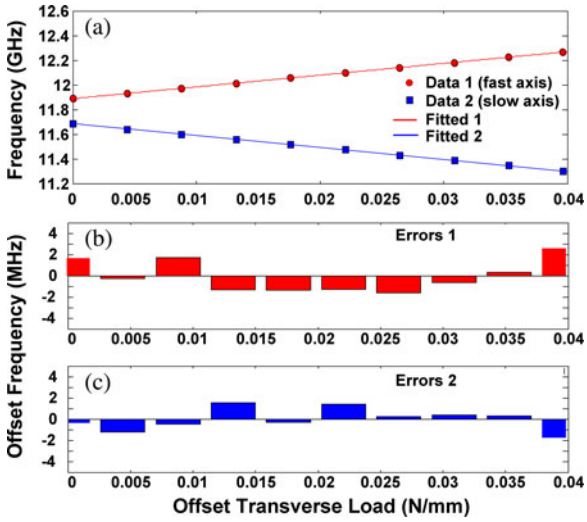

Fig. 11. (a) The measured microwave frequencies versus the transverse load along the fast axis (data 1) and slow axis (data 2). (b) The errors between the measured frequencies and the linearly fitted curve along the fast axis of the PM-PSFBG. (c) The errors between the measured frequencies and the linearly fitted curve along the slow axis of the PM-PSFBG.

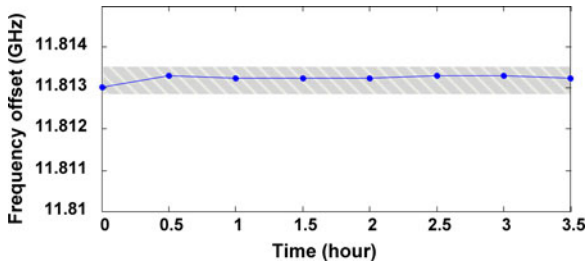

Fig. 12. Stability test result: frequency measurement with 0.5 h interval for a temporal duration of 3.5 h.

According the theoretical analysis in Section II-D, the frequency of the beat note is linearly proportional to the load applied to the fiber with a given angle between the force direction and the principal axis. The microwave frequency with the force applied along either the slow or the fast axis of the PM-PSFBG is measured. To do so, we first apply the force along the slow axis of the PM-PSFBG. By increasing the force with a constant force increment of 0.00441 N/mm, the frequencies are measured and shown in Fig. 11(a) as solid squares. A linearly fitted curve is also shown. Then, we apply the force along the fast axis of the PM-PSFBG. Again, the force is increased with a constant force increment of 0.00441 N/mm. The frequencies are measured and shown in Fig. 11(a) as solid circles. The frequency separation at a zero load is caused by the initial load applied to the PM-PSFBG. By using the typical values of a silica fiber at a wavelength of 1550 nm: $n_0 = 1.467$, $p_{11} = 0.12$, $p_{12} = 0.27$, $\nu_p = 0.17$, $E = 7.6 \times 10^4$ N/mm and the radius of optical fiber $r = 62.5$ μm, the theoretical sensitivity of the sensor is calculated to be 9.9 GHz/(N/mm), while the linearly fitted slopes are $+9.7573$ and -9.7350 GHz/(N/mm) for the force applied along the fast and the slow axes, respectively. A good agreement between the theoretical and the experimental results is reached. The errors between the measured frequencies and the linearly fitted values, shown in Fig. 11(b) and (c), are all smaller than 3.08 MHz, which is within one FSR of the OEO loop. This illustrates that the microwave signal will oscillates at the discrete frequencies determined by the FSR which is close to the theoretical value where only the birefringence is taken into consideration. Therefore, the resolution of the system can be defined by the FSR of the OEO loop. The resolution of the system is calculated as 3.1566×10^{-4} N/mm or 3.1638×10^{-4} N/mm, corresponding the FSR of 3.08 MHz, for the force applied along, respectively, the fast and slow axes in the experiment.

The measurement range of the optical probe can reach 7.5 N/mm determined by the spectral width from the ultra-narrow notch to one edge of its reflection band, which is about 75 GHz. The measurement range is also limited by the bandwidths of the PD, the PM and the EA. In the experiment, the measurement range is ~0.6 N/mm, limited by the bandwidth of the EA (6–18 GHz) and the initial-birefringence-induced offset frequency (11.8 GHz) of the PM-PSFBG.

The stability of the sensor is also studied. To do so, we measure the microwave frequency every half an hour during a 3.5 h period without a load applied to the fiber. This is the condition in which the fiber sensor suffers from the strongest influence from the environment disturbance. As can be seen from the results shown in Fig. 12, the frequency fluctuations are always within 0.5 MHz. Considering the FSR of the OEO loop is 3.08 MHz and the bandwidth of the equivalent MWP filter is 10 MHz, thus the filter is able to select a single mode to guarantee a single mode operation. In the experiment, no mode hoping is observed. The fluctuations are mainly caused by the environmental disturbance such as vibrations, air turbulence and temperature fluctuations. In the experiment, all fibers including the PM-PSFBG are exposed to the environment with no packaging. The errors can be reduced is the system is well packaged with temperature control.

In the experiment, the PM-PSFBG is fabricated using a PMF, which has an initial birefringence, leading to a non-zero beat frequency at 11.8 GHz. If the PM-PSFBG is replaced by a PSFBG written in a fiber with a much smaller initial birefringence, a much lower beat frequency will be generated. Thus, the interrogation system can be implemented using low-frequency electronic components with reduced cost.

IV. Conclusion

A novel dual-wavelength fiber ring laser with improved lasing stability realized through the use of an injection-coupled OEO was proposed and demonstrated, and its application to transverse load sensing was studied. The key mechanism to increase the lasing stability is to use the microwave signal from the OEO to injection lock the dual wavelengths of the fiber ring laser. A theoretical analysis was performed, which was verified by an experiment.

Thanks to the significantly increased stability, the fiber ring laser is an excellent candidate for sensing applications. In the experiment, a transverse load was applied to the PM-PSFBG, and the microwave frequencies for different transverse load were measured. The experimental results showed that the theoretical and the experimental results agreed well. The sensitivity of the transverse load sensor was measured as high as +9.754 and −9.735 GHz/(N/mm), when the load was applied along the fast and slow axes, respectively. The high frequency purity and stability of the generated microwave signal enabled very reliable and high accuracy measurement and the time-domain frequency interrogation allowed the system to operate at an ultra-high speed.

References

[1] F. Zhang, P. L. Chu, R. Lai, and G. R. Chen, "Dual-wavelength chaos generation and synchronization in erbium-doped fiber lasers," *IEEE Photon. Technol. Lett.*, vol. 17, no. 3, pp. 549–551, Mar. 2005.

[2] L. Morvan, N. D. Lai, D. Dolfi, J. P. Huignard, M. Brunel, F. Bretenaker, and A. Le Floch, "Building blocks for a two-frequency laser lidar-radar: A preliminary study," *Appl. Opt.*, vol. 41, no. 27, pp. 5702–5712, Sep. 2002.

[3] T. Suzuki, T. Yazawa, and O. Sasaki, "Two-wavelength laser diode interferometer with time-sharing sinusoidal phase modulation," *Appl. Opt.*, vol. 41, no. 10, pp. 1972–1976, Apr. 2002.

[4] A. M. R. Pinto, O. Frazão, J. L. Santos, M. Lopez-Amo, J. Kobelke, and K. Schuster, "Interrogation of a suspended-core Fabry–Perot temperature sensor through a dual wavelength raman fiber laser," *J. Lightw. Technol.*, vol. 28, no. 21, pp. 3149–3155, Nov. 2010.

[5] X. F. Chen, Z. C. Deng, and J. P. Yao, "Photonic generation of microwave signal using a dual-wavelength single-longitudinal-mode fiber ring laser," *IEEE Trans. Microw. Theory Tech.*, vol. 54, no. 2, pp. 804–809, Feb. 2006.

[6] S. Rota-Rodrigo, L. Rodriguez-Cobo, M. A. Quintela, J. M. Lopez-Higuera, and M. Lopez-Amo, "Dual-wavelength single-longitudinal mode fiber laser using phase-shift Bragg gratings," *IEEE J. Sel. Topics Quantum Electron.*, vol. 20, no. 5, pp. 1–5, Sep.–Oct. 2014.

[7] S. Feng, O. Xu, C. Lu, S. Lu, T. Ning, and S. Jian, "Switchable single-longitudinal-mode dual-wavelength erbium-doped fiber ring laser based on one polarization-maintaining fiber Bragg grating incorporating saturable absorber and feedback fiber loop," *Opt. Commun.*, vol. 282, no. 11, pp. 2165–2168, Jun. 2009.

[8] Y. T. Dai, X. F. Chen, J. Sun, Y. Yao, and S. Z. Xie, "Dual-wavelength DFB fiber laser based on a chirped structure and the equivalent phase shift method," *IEEE Photon. Technol. Lett.*, vol. 18, no. 18, pp. 1964–1966, Sep.-Oct. 2006.

[9] J. Sun, Y. T. Dai, Y. J. Zhang, X. F. Chen, and S. Z. Xie, "Dual-wavelength DFB fiber laser based on unequalized phase shifts," *IEEE Photon. Technol. Lett.*, vol. 18, no. 23, pp. 2493–2495, Nov.-Dec. 2006.

[10] X. Y. He, X. Fang, C. R. Liao, D. N. Wang, and J. Q. Sun, "A tunable and switchable single-longitudinal-mode dual-wavelength fiber laser with a simple linear cavity," *Opt. Exp.*, vol. 17, no. 24, pp. 21773–21781, Nov. 2009.

[11] L. Gao, L. Chen, L. Huang, S. C. Liu, Z. W. Yin, and X. F. Chen, "Simultaneous Measurement of Strain and Load Using a Fiber Laser Sensor," *IEEE Sensors J.*, vol. 12, no. 5, pp. 1513–1517, May 2012.

[12] B. O. Guan, L. Jin, Y. Zhang, and H. Y. Tam, "Polarimetric heterodyning fiber grating laser sensors," *J. Lightw. Technol.*, vol. 30, no. 8, pp. 1097–1112, Apr. 2012.

[13] M. Jones, "Structural-health monitoring: A sensitive issue," *Nature Photon.*, vol. 2, no. 2, p. 153-154, Mar. 2008.

[14] H. L. Guo, G. Z. Xiao, N. Mrad, and J. P. Yao, "Fiber optic sensors for structural health monitoring of air platforms," *Sensors*, vol. 11, no. 4, pp. 3687–3705, Apr. 2011.

[15] E. Pinet, "Medical applications: Saving lives," *Nature Photon.*, vol. 2, no. 2, pp. 150–152, Mar. 2008.

[16] H. Nakstad and J. T. Kringlebotn, "Oil and gas applications: Probing oil fields," *Nature Photon.*, vol. 2, no. 2, pp. 147–149, Mar. 2008.

[17] N. Imoto, N. Yoshizawa, J. I. Sakai, and H. Tsuchiya, "Birefringence in single-mode optical fiber due to elliptical core deformation and stress anisotropy," *IEEE J. Quantum Electron.*, vol. QE-16, no. 11, pp. 1267–1271, Nov. 1980.

[18] L. Y. Shao, A. Laronche, M. Smietana, P. Mikulic, W. J. Bock, and J. Albert, "Highly sensitive bend sensor with hybrid long-period and tilted fiber Bragg grating," *Opt. Commun.*, vol. 283, no. 13, pp. 2690–2694, Jul. 1, 2010.

[19] R. Ulrich, S. C. Rashleigh, and W. Eickhoff, "Bending-induced birefringence in single-mode fibers," *Opt. Lett.*, vol. 5, no. 6, pp. 273–275, Jun. 1980.

[20] H. Chi, X. M. Tao, D. X. Yang, and K. S. Chen, "Simultaneous measurement of axial strain, temperature, and transverse load by a superstructure fiber grating," *Opt. Lett.*, vol. 26, no. 24, pp. 1949–1951, Dec. 2001.

[21] M. LeBlanc, S. T. Vohra, T. E. Tsai, and E. J. Friebele, "Transverse load sensing by use of pi-phase-shifted fiber Bragg gratings," *Opt. Lett.*, vol. 24, no. 16, pp. 1091–1093, Aug. 1999.

[22] F. Kong, W. Li, and J. Yao, "Transverse load sensing based on a dual-frequency optoelectronic oscillator," *Opt. Lett.*, vol. 38, no. 14, pp. 2611–2613, Jul. 2013.

[23] F. Zhang and J. W. Y. Lit, "Temperature and strain sensitivity measurements of high-birefringent polarization-maintaining fibers," *Appl. Opt.*, vol. 32, no. 13, pp. 2213–2218, May 1993.

[24] Y. Zhang, B. O. Guan, and H. Y. Tam, "Characteristics of the distributed Bragg reflector fiber laser sensor for lateral force measurement," *Opt. Commun.*, vol. 281, no. 18, pp. 4619–4622, Sep. 2008.

[25] H. Y. Fu, X. W. Shu, C. B. Mou, L. Zhang, S. L. He, and I. Bennion, "Transversal loading sensor based on tunable beat frequency of a dual-wavelength fiber laser," *IEEE Photon. Technol. Lett.*, vol. 21, no. 14, pp. 987–989, Jul. 2009.

[26] W. Z. Li, M. Li, and J. P. Yao, "A narrow-passband and frequency-tunable microwave photonic filter based on phase-modulation to intensity-modulation conversion using a phase-shifted fiber Bragg grating," *IEEE Trans. Microw. Theory Tech.*, vol. 60, no. 5, pp. 1287–1296, May 2012.

[27] W. Z. Li and J. P. Yao, "A wideband frequency tunable optoelectronic oscillator incorporating a tunable microwave photonic filter based on phase-modulation to intensity-modulation conversion using a phase-shifted fiber Bragg grating," *IEEE Trans. Microw. Theory Tech.*, vol. 60, no. 6, pp. 1735–1742, Jun. 2012.

[28] J. T. Kringlebotn, W. H. Loh, and R. I. Laming, "Polarimetric Er3 + -doped fiber distributed-feedback laser sensor for differential pressure and force measurements," *Opt. Lett.*, vol. 21, no. 22, pp. 1869–1871, Nov. 15, 1996.

Fanqi Kong (S'13) received the B.Eng. degree in optoelectronic information engineering from the Huazhong University of Science and Technology, Wuhan, China, in 2012. He is currently working toward the M.A.Sc. degree in the School of Electrical Engineering and Computer Science, University of Ottawa, Ottawa, ON, Canada.

His current research interests include photonic generation of microwave signals and applications in sensing systems.

Bruno Romeira (M'13) received the five-year Diploma degree in physics and chemistry from the University of the Algarve, Faro, Portugal, in 2006, where he also received the Ph.D. degree in physics (*Summa Cum Laude*) and the title of European Ph.D., jointly with the University of Glasgow, Glasgow, U.K., and the University of Seville, Sevilla, Spain, in 2012.

He is currently engaged in a Postdoctoral Fellowship Program at the Center of Electronics Optoelectronic and Telecommunications, Department of Physics, University of the Algarve, and at the Microwave Photonics Research Laboratory, University of Ottawa, Canada, as a visiting Postdoctoral Fellow. His research interests include several disciplines in applied physics and engineering, which include semiconductor physics, solid-state electronics, and optoelectronic. He is also interested in complex systems, chaos, and synchronization for novel applications in information and communication technologies.

Dr. Romeira received the "Young Researchers Incentive Programme" award from the Calouste Gulbenkian Foundation, Portugal, in 2009, and the "IEEE Photonics Society Graduate Student Fellowship" (2011), from the IEEE Photonics Society, USA. His Ph.D. thesis entitled "Dynamics of Resonant Tunneling Diode Optoelectronic Oscillators" was awarded the "Best Ph.D. Thesis in Optics and Photonics in Portugal in 2012" by the Portuguese Society of Optics and Photonics.

Jiejun Zhang (S'12) received the B.S. degree from the Harbin Institute of Technology, Harbin, China, in 2006, and the M.S. degree from the Huazhong University of Science and Technology, Wuhan, China, in 2012. He is currently working toward the Ph.D. degree in electrical engineering and computer science at the Microwave Photonics Research Laboratory, University of Ottawa, Ottawa, ON, Canada.

His research interests include photonic generation of microwave arbitrary waveforms, photonic processing of microwave signals and fiber optic sensing technology.

Wangzhe Li (S'08) received the B.E. degree in electronic science and technology from Xi'an Jiaotong University, Xi'an, China, in 2004, the M.Sc. degree in optoelectronic and electronic science from Tsinghua University, Beijing, China, in 2007, and the Ph.D. degree in electrical engineering from the University of Ottawa, Ottawa, ON, Canada, in 2013.

He is currently a Postdoctoral Researcher with the Microwave Photonics Research Laboratory, School of Electrical Engineering and Computer Science, University of Ottawa. His current research interests include photonic generation of microwave and Terahertz signals.

Dr. Li received a 2011 IEEE Microwave Theory and Techniques Society Graduate Fellowship and 2011 IEEE Photonics Society Graduate Fellowship.

Jianping Yao (M'99 – SM'01 – F'12) received the Ph.D. degree in electrical engineering from the Université de Toulon, Toulon, France, in December 1997.

He joined the School of Electrical Engineering and Computer Science, University of Ottawa, Ottawa, ON, Canada, as an Assistant Professor in 2001, where he became an Associate Professor in 2003 and a Full Professor in 2006. He was appointed the University Research Chair in Microwave Photonics in 2007. From July 2007 to June 2010, he was the Director of the Ottawa-Carleton Institute for Electrical and Computer Engineering. Prior to joining the University of Ottawa, he was an Assistant Professor in the School of Electrical and Electronic Engineering, Nanyang Technological University, Singapore, from 1999 to 2001. He has published more than 450 papers, including more than 260 papers in peer-reviewed journals and 190 papers in conference proceedings.

Prof. Yao is a Topical Editor for Optics Letters. He is a Chair of numerous international conferences, symposia, and workshops, including the Vice-TPC Chair of the 2007 IEEE Microwave Photonics Conference, TPC Cochair of the 2009 and 2010 Asia-Pacific Microwave Photonics Conferences, TPC Chair of the high-speed and broadband wireless technologies subcommittee of the 2009 – 2012 IEEE Radio Wireless Symposia, TPC Chair of the microwave photonics subcommittee of the 2009 IEEE Photonics Society Annual Meeting, TPC Chair of the 2010 IEEE Microwave Photonics Conference, and General Cochair of the 2011 IEEE Microwave Photonics Conference. He received the 2005 International Creative Research Award at the University of Ottawa. He received the 2007 George S. Glinski Award for Excellence in Research. He was selected to receive an inaugural OSA Outstanding Reviewer Award in 2012. He serves as an IEEE Distinguished Microwave Lecturer for 2013 – 2015. He is a registered Professional Engineer of Ontario. He is a Fellow of the Optical Society of America and the Canadian Academy of Engineering.